AD-A115 879 LAWRENCE LIVERMORE NATIONAL LAB LIVERMORE CA F/G 20/4
COMPLIANT MATERIAL COATING RESPONSE TO A TURBULENT BOUNDARY LAY--ETC(U)
MAY 82 A C BUCKINGHAM, R C CHUN, R L ASH W-7405-ENG-48
UNCLASSIFIED UCRL-86937 NL

END
DATE FILMED
7-82
DTIC

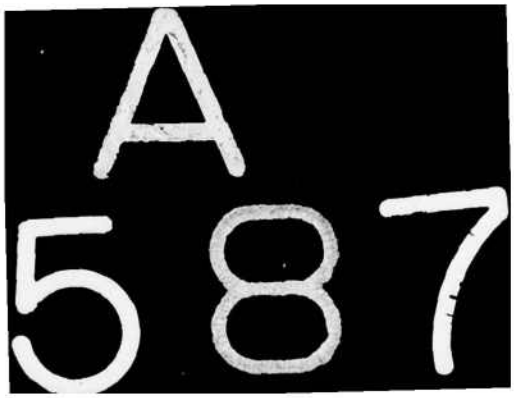
A
587

UCRL-86937
PREPRINT

COMPLIANT MATERIAL COATING RESPONSE TO A TURBULENT BOUNDARY LAYER

A. C. Buckingham and R. C. Chun
University of California, Lawrence Livermore National Laboratory

R. L. Ash and M. Khorrami
Old Dominion University, Norfolk, Virginia

This paper was prepared for presentation/publication as AIAA Paper No. 82-1027 at the AIAA/ASME 3rd Joint Thermophysics, Fluids, Plasma & Heat Transfer Conference, June 7-11, 1982, St. Louis, Mo.

May 1982

COMPLIANT MATERIAL COATING RESPONSE TO A TURBULENT BOUNDARY LAYER*

Alfred C. Buckingham,** Ramsey C. Chun***
University of California, Lawrence Livermore National Laboratory
Livermore, California 94550

Robert L. Ash,† Mehdi Khorrami††
Old Dominion University
Norfolk, Virginia 23508

Abstract

We describe results of transient two-dimensional finite element computations used to simulate elastic and visco-elastic surface response to the stress generated by the surface turbulent boundary layer in water. We are characterizing the temporal and spatial response of soft, pliable surface coating materials such as natural rubbers, artificially treated rubber-like compounds, and cured polymeric gels. We examine a variety of coatings from stacked homogeneous layers to internally structured layers with open and fluid filled cells or with directional ribs and channels. In addition, we examine non-linear visco-elastic loss characteristics and time-dependent influences on material response. Our goal is identifying drag and characterizing the most important dynamic material properties to achieve this end. Two dimensional transient numerical computations are applied to simulate the space and time random scalar pressures which excite the material response.

I. Introduction

Our investigation focuses on compliant coatings which exhibit favorable dynamic response relative to critical turbulent boundary layer motions. Favorable response refers to surface motions which may reduce or cancel the boundary layer motions and consequently reduce skin friction drag. The characterization of fluid-solid interface dynamics with relation to material properties and identification of the fundamental fluid/solid dynamic coupling mechanisms with a potential for reducing skin friction drag are the basic purposes of this research. Emphasis is placed on materials and coatings whose compliant material properties and response characteristics can be altered to respond to the turbulence by modifying internal structure, or composite material stiffness, or dynamically altering viscous filler properties or by internal heating. Such coatings may be effective over a broad range of flow conditions. Our analysis is specifically directed to drag reduction on coated surfaces moving in water.

Post World War II attention on compliant coated drag reduction possibilities was stimulated by study of the swimming efficiency of mammals, particularly porpoises. One of the early post World War II investigations, in which trial coatings were devised, was apparently based on study of the porpoise skin surface and sub-surface bone, cartilage, fat, and vascular composition and structure. These coatings were developed and tested in the United States by M. O. Kramer in the 1950's and 1960's.[1,2] Unfortunately, the experimental results which indicated that significant drag reduction could be achieved using a combination of viscoelastic layered materials and internal structures, were never independently and reproducibly verified. The issue remains open.

In the United States, subsequent comprehensive studies on compliant surface drag reduction and materials characterization were conducted and reported by researchers at NASA Langley in the 1970's.[3,4,5] Suggestions were made about the mechanisms by which transitional boundary layer stabilization and turbulent boundary layer intensity reduction may take place. The notions advanced, generally focus on modulation of energetic, transient boundary layer relatively large scale structural features which have been observed in comparatively recent turbulent boundary layer experiments. Presumably the most probable drag reducing dynamic fluid solid coupling mechanisms may be suggested by these experiments and further developed by theoretical analysis and simulation prior to verification by carefully defined and conducted experiments.

Computer simulations of the complicated boundary layer flow and instability evolution adjacent to initially prescribed deformed surfaces or surface motions have been presented by Orszag.[9,10,11] In these numerical simulations experimental evidence was useful in suggesting simplications to the computational model. By modeling certain, almost periodic, features and by special care with respect to the numerical method applied, pseudo-spectral computations of the generalized Navier-Stokes model solutions are obtained. These solutions represent the most sophisticated turbulence simulations adjacent to arbitrarily deformed surfaces. They form an accurate basis for analysis, provided sufficient attention is given to computational efficiency, uniform validity, and a clearly defined limit to application range.

We make frequent use of the results and interpretations from these experimental and computational studies in our computational efforts at identifying potential compliant surface materials and drag reducing coatings. The most promising are projected as candidates for later experimental

---

*Work performed under the auspices of the U.S. Department of Energy by Lawrence Livermore National Laboratory under contract #W-7405-Eng-48 and supported by the Department of the Navy, Office of Naval Research under contract #N000-14-82-F-0010.

**Physicist, Fluid Dynamics, H-Division, Physics Dept., Associate Fellow AIAA.
***Research Engineer, Engineering Mechanics, Nuclear Test Engineering Division, Engr. Dept.
†Professor, Mechanical Engineering & Mechanics Dept.
††Graduate Student, Mechanical Engineering & Mechanics Dept.

study. Some of our preliminary results, appearing here for background information, have been presented within the year.[12]

II. Procedure

To develop realistic, experimentally verified turbulent excitation pressure space and time histories we make use of one of our co-author's (Ash) two-dimensional and three-dimensional Monte-Carlo time dependent turbulent pressure simulations to generate our dynamic loading functions.[13] Subsequently, we plan to explore the actual coupling mechanism(s) using the general numerical solutions of the turbulent Navier-Stokes equations through application of Orszag's pseudo-spectral method.[9-11,16] In this paper we restrict our discussion to an intermediate phase: systematical materials property and response characterization. We emphasize, at this time, thorough evaluation of compliant materials, special internal structures, and passive response and motion modulation. For this we apply the Ash code model Monte Carlo pressure simulations.[13]

We consider a flat plate, with zero pressure gradient immersed immediately below the surface in sea water. We examine conditions over a range of specified steady state free stream velocities. The Ash procedure[13] generates a modeled scalar turbulent boundary randomly fluctuating surface pressure using a quasi-Monte-Carlo method to develop the random time histories at preselected time intervals and spatial locations. The turbulent pressure development is considered tripped at a selected upstream position by a finite (mm) wire transition trip. A hypothetical development length, 50 wire diameters downstream is estimated for initiation of the fully developed turbulent boundary layer. This defines development length and point of origin for the fully developed boundary layer fluctuating pressure simulations generated by the Ash code. The Ash code results have been shown to model fluctuating pressures and scale features of the boundary layer in close agreement with the experimental observations of Bull[14] and of Bull, Thomas.[15] Nevertheless, this is a pressure model only. Convection and convection-dominated burst-streak and upthrust vorticity generation features are separately imposed using observations based on the Offen-Kline observations associated with unsteady characteristics of the turbulent boundary layer.[8]

Specifically, we adopt for the present calculation the Offen-Kline implications of the dependence of the spread between burst events as proportional to the inner boundary layer (wall region) variables,

$$\Delta x = u_\sigma \, \Delta t \tag{1}$$

where Δx is the spatial distance between burst events, Δt is the time interval and u_σ is the shear velocity given by the wall shear, Σ_ω, in accordance with,

$$u_\sigma = \sqrt{\Sigma_\omega/\rho}\,\Big|_{y=0} \tag{2}$$

where ρ is the fluid density and y is the normal coordinate displacement from the wall surface through the boundary layer. Incompressible, turbulent boundary layer solutions are obtained at the start, to establish the necessary estimated values of local displacement thickness, δ_2, wall shear, Σ_ω, root mean square pressure

$$\langle p' \rangle \tilde{\sim} 3.0 * \Sigma_\omega \, . \tag{3}$$

And time scales for unsteady burst growth, propogation and decay. The entire burst evolution is assumed convected with the mean flow at a high but constant speed proportional to the outer edge velocity, viz.

$$u_c \tilde{=} 0.8 \, U_\infty \tag{4}$$

Experiments conducted at the NBS and Naval Research Laboratories on promising coatings will verify their performance. They will also provide information for the development and subsequent analysis of material properties and the crucial features of the interactive coupling model.

Next, we apply a discretized procedure to numerically simulate the response of composite materials and structures. To accurately follow high frequency motions, in a practical computation, both implicit and explicit two-dimensional and three-dimensional LLNL finite element codes of Hallquist are used.[17,18]

Among the principal finite element code features consistently used in the present analysis, is the facility for treating slide lines (or in the 3D version sliding surfaces) between unlike materials or at geometric discontinuities. The interface between the PVC and Neoprene layers, for example is treated by a range of options from friction to free sliding constraints which remove the ambiguity associated with discontinuous material properties and associated erroneous discontinuities in the continuum description of the dynamic stress tensor field.

Generally, the unsteady dynamical problem is formulated in a lumped mass matrix form as a perturbation to equilibrium static equations. Unsteady dynamics are a perturbation to the equilibrium system which is relaxed in the implicit NIKE code version to a new equilibrium state or time marched in the explicit DYNA code version to the next advanced time step. The lumped mass matrix form is written

$$\underset{\sim}{M}\ddot{\underset{\sim}{d}}^{n+1} + \underset{\sim}{D}(\underset{\sim}{d}^n + \alpha\Delta\underset{\sim}{d})\,\dot{\underset{\sim}{d}}^{n+1} + \underset{\sim}{K}_T(\underset{\sim}{d}^n + \alpha\Delta\underset{\sim}{d}^*)\,\Delta\underset{\sim}{d}_0$$

$$= \underset{\sim}{P}(\underset{\sim}{d}^n)^{n+1} - \underset{\sim}{F}(\underset{\sim}{d}^n) \tag{5}$$

The first term represents the nodel mass acceleration acting on a consistent lumped mass matrix, $\underset{\sim}{M}$. Single and double dots over the deformation matrix elements, $\underset{\sim}{d}$, refer to 1st and 2nd derivatives with respect to time. The operator matrix, $\underset{\sim}{D}$, is a Rayleigh damping matrix,

$$\underset{\sim}{D} \equiv \alpha_d \underset{\sim}{M} + \beta_d \underset{\sim}{K}_T \, , \tag{6}$$

where $\underset{\sim}{K}_T$, is the material property dependent symmetric positive definite stiffness matrix, $\underset{\sim}{P}$ represents the external loads vector and $\underset{\sim}{F}$ is the stress divergence vector centered at time "n".

The constants α_d and β_d are user defined at initiation of a specific problem. The term $\tilde{d}^*$ represents the estimated displacement vector associated with elemental loads and acceleration at the start of an iteration. In addition to the slide line and slide surface features, the freedom to apply body force or concentrated nodal loads, pressure boundary conditions, shear boundary conditions, displacement boundary conditions all within a self consistent Jaumann stress rate formulation, serve useful purposes in our applications. In our simulations we are specifically concerned with composite structures of arbitrary scale size in dynamic simulations with problem defined time constants.

The material models available include elastic, orthotropic elastic, elastic-plastic and linear visco-plastic. The first and last two are of particular interest to us in our application.

These permit modeling of variable composite material properties and constitutive relations, and modeling of the internally structured compliant surface coatings, such as those with air gaps, water passages, and rigid reinforcing stubs. These interior structures, in some cases, are found to effectively shorten the characteristic response wavelength. Addition of heat to "tune" the material elastic moduli, and specified internal fluid pressures associated with internal cell-to-cell liquid flow (which modifies both structural stiffness and damping) are also modeled, quite generally. The present finite element results are for pure elastic and damped viscoelastic modeled composite materials in transient, plane two-dimensional strain. The three-dimensional surface is considered composed of streamwise infinitesimally thin strips excited by the two dimensional transient random pressure oscillations. We examine the displacement response of various surface materials, composites and structures. Boundary conditions include both clamped and roller end conditions on the strip with a rigid, non-yielding lower surface. Full three dimensional driven surfaces are simulated in later calculations, together with numerical simulations of the complete Navier-Stokes equations of motion following the pseudo-spectral Orszag procedure. This work in current progress is directed to definition and evaluation of the full fluid-to-solid-to-fluid coupling and will be described in later publications.

III. Results

We present preliminary results of our previous computations and analysis[12] to assist description of our numerical procedures and the physical interpretation of our currently available results with respect to potential drag reduction.

Figures 1 and 2 show elastic response of indicated materials as characterized by response amplitude and circular frequency, respectively. Both sets of calculations were made for zero immersion depth ocean surface (Z = 0) motion. The solid curves are the response envelopes for the indicated speeds: 10, 20, and 30 m/s. The dashed curves intersecting are the response intercepts for the specified materials: natural rubber, neoprene and plastisol gel (PVC). The amplitude response, d, Fig. 1 is ratioed to a critical boundary layer dimension, δ_2, (displacement thickness) relative to dimensions of potentially unstable motions of the wall. The rms turbulent pressure fluctuation $\langle p' \rangle$ is ratioed to the Young's modulus (E) of the materials in these illustrations.

Figure 3 illustrates configuration, computational geometry, and displacement response results for elastic analysis of homogeneous layers of PVC on neoprene and the reverse ordering of the layers, neoprene on PVC. Pure sinusoidal excitation pressures were used for these preliminary studies. We found that in this simple elastic limit the displacements, d, ratioed to the depth of material layer, h, is functionally characterized by a dimensionless group relationship,

$$\frac{d}{h} = \text{constant} * \frac{\langle p' \rangle}{E} (1-\bar{\nu}^2) \left(\frac{b}{h}\right)^4 f\left(\frac{\omega}{\omega_0}\right) . \qquad (7)$$

Here $\bar{\nu}$ is the composite, effective Poisson's ratio, b is the effective pressure patch breadth, ω_0 is the characteristic natural frequency of the material layer. The layers show the normal tendency to amplitude divergence indicated near the characteristic frequency, ω_0. The softer PVC on the upper surface is clearly superior to the opposite arrangement for obtaining the largest amplitude response in material layers. Similar dimensional analysis collapse of the response histories for surface coatings consisting of visco-elastic elements has, so far, been unsuccessful. However, such a characterization is sought from our analysis in order to provide a basis for material and structural characterization when subjected to random turbulent loads.

The non-linear frequency dependence of the shear modulus for one of the materials, "plastisol" (PVC) is shown in Fig. 4. This experimental (dashed curve) material frequency dependence is modeled satisfactorily (solid curve) in the finite element plane strain calculations. The experimental data was provided to us by researchers at the Naval Research Laboratory. Figure 5 shows the relative variation in amplitude response for the viscoelastic, internally structured material coatings possessing internal cells of about 1/3 total coating depth. They are numerically tested with various "fillers" in the open channels. Fillers included tests with void (actually air at 1 atm.), plastisol filler, water, and neoprene filler with the order of response magnitude following the same order as the listed fillers. Voids give the greatest displacement and neoprene filler the least. However, considering both response frequency and amplitude, the visco elastic incompressible fillers are the most promising of the materials simulated in these numerical tests.

Three classes of materials, geometries and structures for compliant coatings are studied here. We examine, in turn, homogeneous multiple material layered coatings, internally structured coatings with imbedded cells or channels filled with visco-elastic incompressible fluid, and a small dimension (2 mm thick) Kramer coating suggested by his later studies.[19]

Figures 6 through 12 summarize our findings on uniformly homogeneous layered structures with 10% PVC plastisol overlaying a neoprene sub-surface layer in a compliant coating over a relatively rigid (aluminum) surface. The geometry and surface deformation pattern (enlarged by the explicit scale factor) is shown at time zero (static) and

three subsequent times, where times are given in sec.

The driving pressure (P_a) time histories at 25%, 50% and 75% stations from the leading edge of the compliant surface are shown in Fig. 7. The corresponding Fourier transformed pressure spectra are shown in Fig. 8. Peak frequency shifts to lower values as the wave train energy is distributed over a larger streamwise dimension and decays with increasing involvement in the modeled boundary layer fluid.

The resulting surface displacement amplitude time histories are shown in Figs. 9 and 10 for free stream speeds of 10 and 30 m/s, respectively. The amplitude spectra are illustrated in Figs. 11 and 12 for the 10 and 30 m/s speeds, respectively. Shifts of the peak amplitude spectra to lower frequency than that for the driving fluid is more pronounced due to larger solid material inertia, rigidity, and dispersive characteristics. From our previous elastic and viscoelastic studies the softest (PVC) materials tested is usually placed on the surface for developing greater response amplitudes.

We simulated both softer and harder surface materials over structured internal layers in coatings depicted in Figs. 13 through 22. Figures 13 and 14 show geometry of the structured layers and deformation of the surface at designated times (sec) for neoprene and PVC surfaces respectively. The flow speed is 30 m/s. Turbulent pressure time histories and pressure spectra are shown for three designated stations in percentage of length from leading edge in Figs. 15 and 16.

The PVC on the upper (fluid-solid contact) surface gives the largest (most promising) displacement amplitudes. However, the frequency of surface motions is somewhat lower for the softer materials, and is probably too low for useful interference with the oscillatory boundary layer structural features. The displacement amplitudes are shown for 10 m/s and 30 m/s in Figs. 17 and 18, respectively while the corresponding amplitude spectra are shown in Figs. 19 and 20. The shift of the peak of the pressure spectra is evidently a function of increasing length of coating as illustrated by the values at the 25%, 50% and 75% stations from the leading edge of the plate model. Also evident is the lower frequency for peak amplitude of response spectra in comparison to the driving spectra shown in Fig. 16. Here again material inertia, stiffness and dispersive characteristics are dominating influences on the fluid to solid coupling dynamics. Significantly more variation in response will be possible by modulation and tuning of the coating structure dimensions and filler characteristics. These variations or permutations are more conveniently conducted on the computer in order to usefully limit and specialize on a few well-defined candidates for subsequent experiments.

Figures 21 and 22 show the response spectra at 10 and 30 m/s, respectively for the same internally structured coatings but with the harder neoprene replacing the softer PVC for the surface layer with the PVC moved to the substrate coating layer position. Amplitudes are significantly reduced with the firmer surface materials. However, the slight shift to higher frequency for peak response spectra is partially modulated by the characteristics of the internal structure and sub-layer material.

Figures 23 through 26 show the latest small scale (higher frequency response) Kramer ribbed structures suggested by his later work.[19] These simulations were made at a lower velocity (1.5 m/s) suggested by his experiments. While the higher frequencies are excited the response amplitudes (micron or less) are negligible for significant boundary layer interference purposes. Figure 23 illustrates the Kramer geometry and deformations at selected times. Figure 24 shows the driving turbulent pressure spectra at 1.5 m/s. Figures 25 and 26 show this Kramer structure response amplitude and response spectra, respectively.

IV. Preliminary Interpretations

In general, the response of all mono or sequentially layered coatings in water parallel the suggestions derived from the gas flow predictions of Bushnell, Hefner and Ash.[5] Specifically unstructured (non-cellular) passive (non-heated, non-driven coatings) unless very thick (two or three times substrate thickness) exhibited little or no amplification modulation of the response from the driving forcing function that was distinct from that of the rigid metal substrate. This reponse dominance by the substrate characteristics, with negligible coating modulation, becomes more pronounced as speed, burst frequency, and simulated depth increased. The preliminary results imply that for phase resonance between forcing oscillation and the coating, the submembrane cavity would have to be filled with an incompressible liquid to prevent deformation extensive enough to completely overwhelm other desirably broad band structural response characteristics.

Inertial contrasts between fluid and solid coating as well as evident solid stiffness significantly reduce the ratio of fluid excitation amplitude to solid response amplitude and increase the phase lag between fluid excitation and solid response. These factors, in conjunction with natural material dispersion, suggest that attainment of simple fluid/solid direct interference coupling is improbable. It further suggests that for potentially effective drag reduction, combinations of structure and materials must be sought that provide multi-modal response to pulsed excitation from the turbulent boundary layer. One seeks, in this way, to enlarge the probability of generating appropriately phase canceling or attenuating surface motions.

V. References

1. M. O. Kramer, "Boundary Layer Stabilization by Distributed Damping", J. Amer. Soc. of Naval Engrs. 72, 1, 25-33 (February 1960).
2. M. O. Kramer, "Dolphin's Secret", The New Scientist, London 7, 181, 1118-1120 (5 May 1960).
3. M. C. Fisher, L. W. Weinstain, R. L. Ash, D. M. Bushnell, "Compliant Wall-Turbulent Skin-Friction Reduction Research", in AIAA Eighth Fluid and Plasma Dynamics Conference (Hartford, Conn., June 16-18, 1975).
4. J. N. Hefner, D. M. Bushnell, R. T. Whitcomb, A. M. Cary, Jr., "Concepts for Aircraft Drag

Reduction", in AGARD/VKI Special Course on Concepts for Drag Reduction (Rhode-St. Genese, Belgium, March 28-April 1, 1979).
5. D. M. Bushnell, J. M. Hefner, R. L. Ash, Phys. of Fluids 20, 531 (1977).
6. R. F. Blackwelder an R. E. Kaplan, in Turbulent Shear Flows, AGARD Conf. Proc. No. 3 (1972).
7. R. F. Blackwelder and R. E. Kaplan, J. Fluid Mech. 76, 86 (1976).
8. G. R. Offen and S. J. Kline, J. Fluid Mech. 70-2, 209 (1975).
9. S. A. Orszag, "Numerical Simulation of Turbulent Flow over a Compliant Boundary", Flow Research Inc., Kent, Wash. Rept. 63, NASA Contractor's Report NASA CR-144981 (February 1976).
10. S. A. Orszag, "Prediction of Compliant Wall Drag Reduction--Part I", Cambridge Hydrodynamics Inc., Cambridge Mass. Report No. 3 (1977).
11. S. A. Orszag, "Prediction of Compliant Wall Drag Reduction--Part II", Cambridge Hydrodynamics Inc., Cambridge Mass., NASA Contractor's Report NASA CR-3071 (1979).
12. A. C. Buckingham and R. C. Chun, "Compliant Coatings" Dynamic Response Modeling, Computations, and Analysis", presented at ONR Compliant Coating Drag Reduction Program Review (Naval Research Laboratory, Washington, D.C., October 14-15, 1981).
13. R. L. Ash, Simulation of Turbulent Wall Pressure, NASA CR-2958 (May, 1978).
14. M. K. Bull, "Wall Pressure Fluctuations Associated with Subsonic Turbulent Boundary Layer Flow", J. Fluid Mech. 28, 719-754 (1967).
15. M. K. Bull and A. S. W. Thomas, "High Frequency Wall Pressure Fluctuations in Turbulent Boundary Layers", Phys. Fluids 19, 597-599 (1976).
16. D. Gottlieb and S. A. Orszag, Numerical Analysis of Spectral Methods, NSF-CBMS Monograph No. 26, SIAM (Philadelphia, PA, 1977).
17. J. O. Hallquist, "NIKE2D: An Implicit, Finite Deformation, Finite-Element Code for Analyzing the Static and Dynamic Response of Two-Dimensional Solids", Lawrence Livermore National Laboratory, Livermore, CA Report UCRL-52678 (March 3, 1979).
18. J. O. Hallquist, "Preliminary User's Manual for DYNA3D and DYNAP (Nonlinear Dynamic Analysis of Solids in Three Dimensions)", Lawrence Livermore National Laboratory, Livermore, CA Report UCID-17268, Rev. 1 (October 1979).
19. M. L. Kramer, "Improved Ribbed Coatings", unpublished report and figures (1966).

Acknowledgements

The authors acknowledge, with pleasure, the support, encouragement and stimulating discussions with Mike Reischmann of ONR and Jack Hansen of NRL. We are also pleased to mention several thought provoking discussions on the coupling mechanisms with Dennis Bushnell and clarification of the Ash code logic with Balasubramanian of NASA Langley. Our thanks and acknowledgement is also extended to our LLNL colleagues: Lew Glenn for helpful discussions on the fluid to solid interaction formulation, JoAnne Levatin and John French for their perseverance in programming and debugging on CRAY I, CDC 7600, and PRIME 750 computers and to Kathy Smith who prepared thi script with characteristically professio curacy and dispatch.

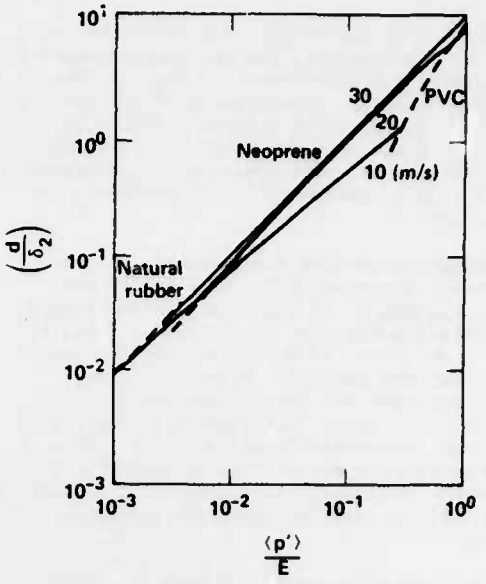

Fig. 1 Elastic theory response amplitudes for selected coating materials as a function of rms pressure.

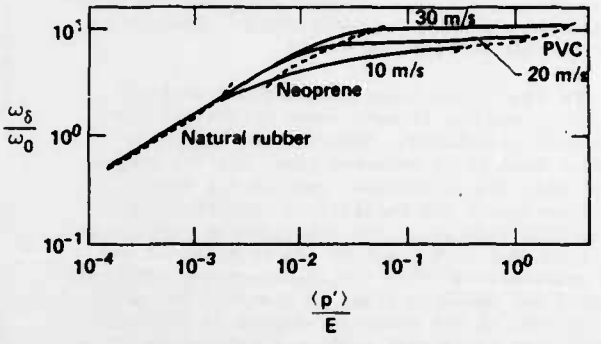

Fig. 2 Elastic theory response frequencies for selected coating materials as a function of rms pressure.

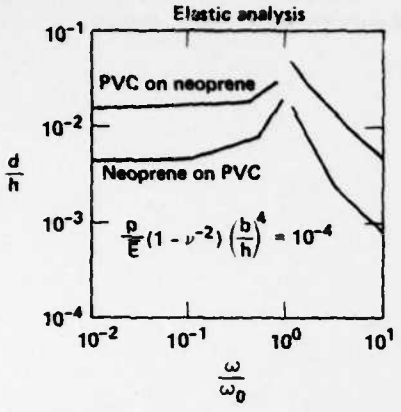

Fig. 3 Characteristics of elastic response for low moduli surface and substrate coating layers.

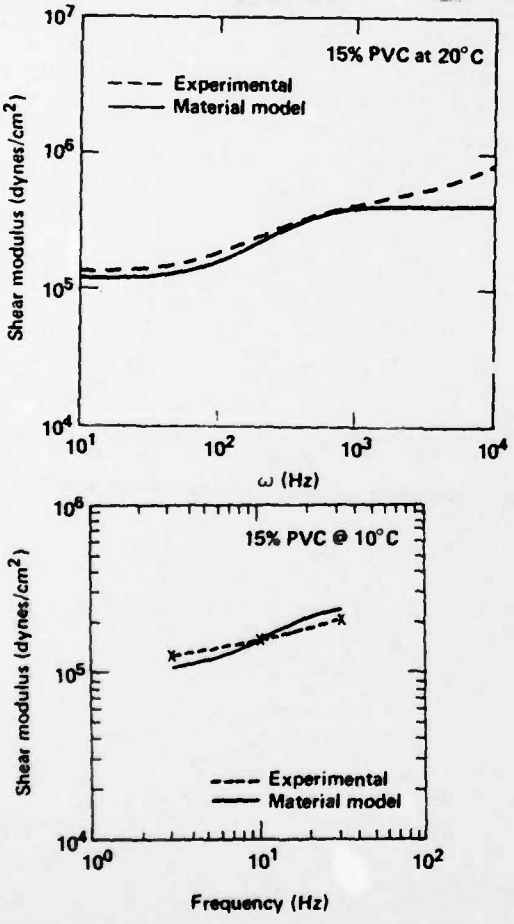

Fig. 4 Viscoelastic PVC shear modulus as a function of applied frequency.

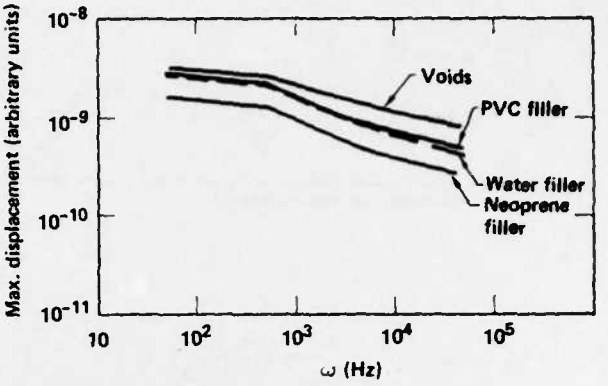

Fig. 5 Viscoelastic displacement response for internally ribbed structures with selected filler materials.

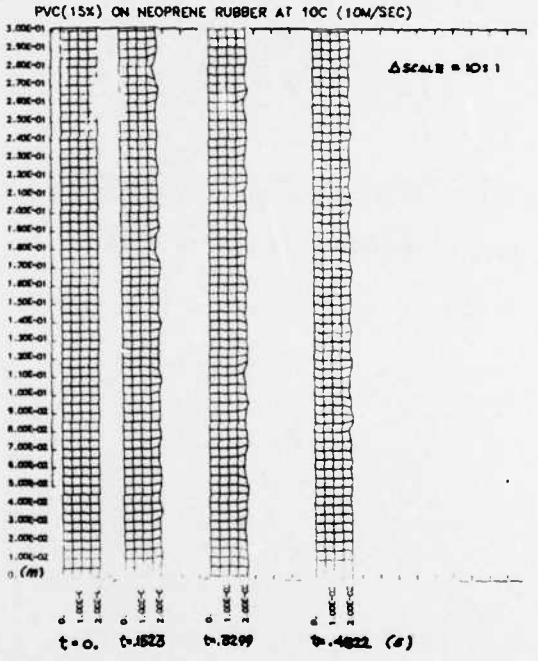

Fig. 6 Uniformly layered geometry and modeled turbulent surface deformations at 10 m/s.

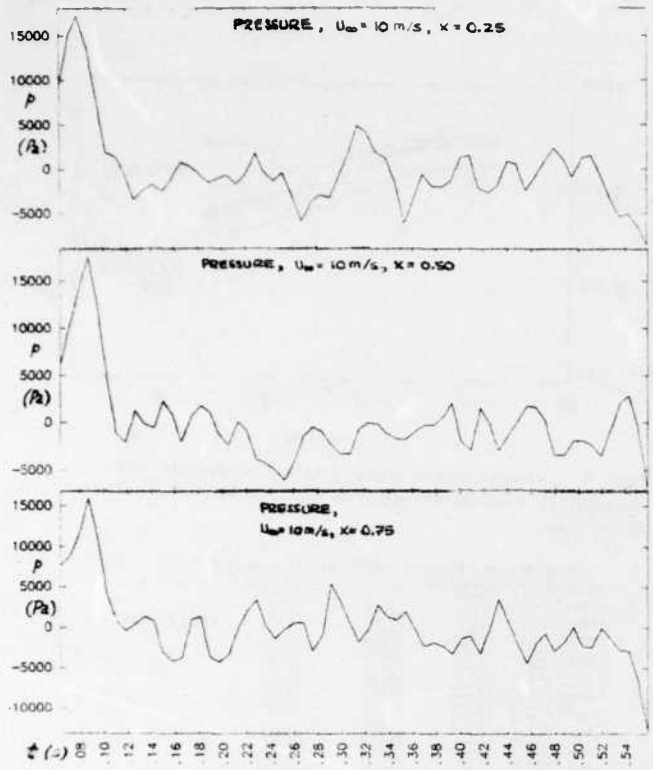

Fig. 7 Turbulent pressure at 10 m/s.

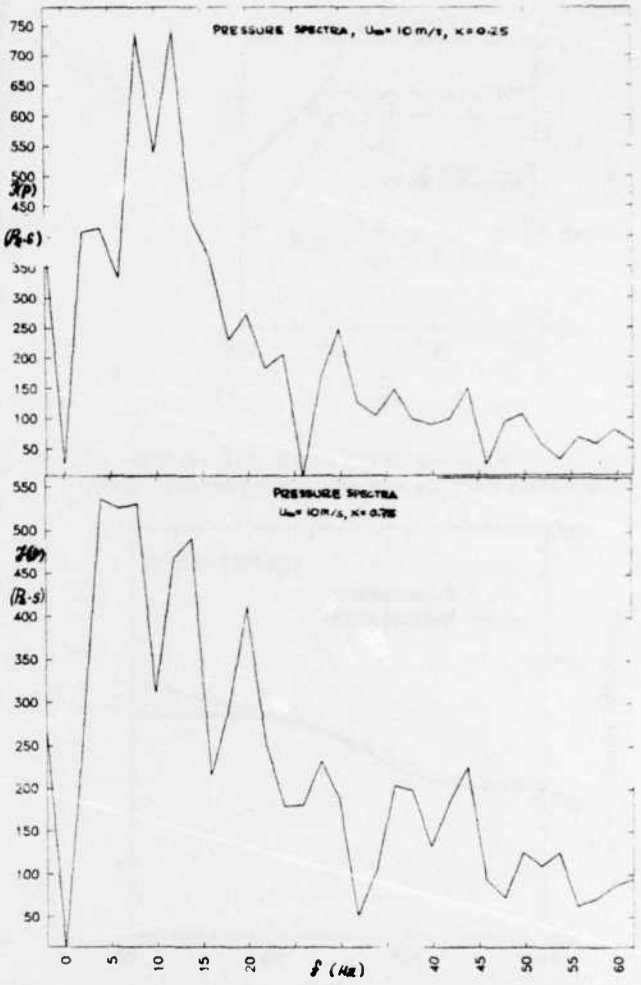

Fig. 8 Turbulent pressure spectra at 10 m/s.

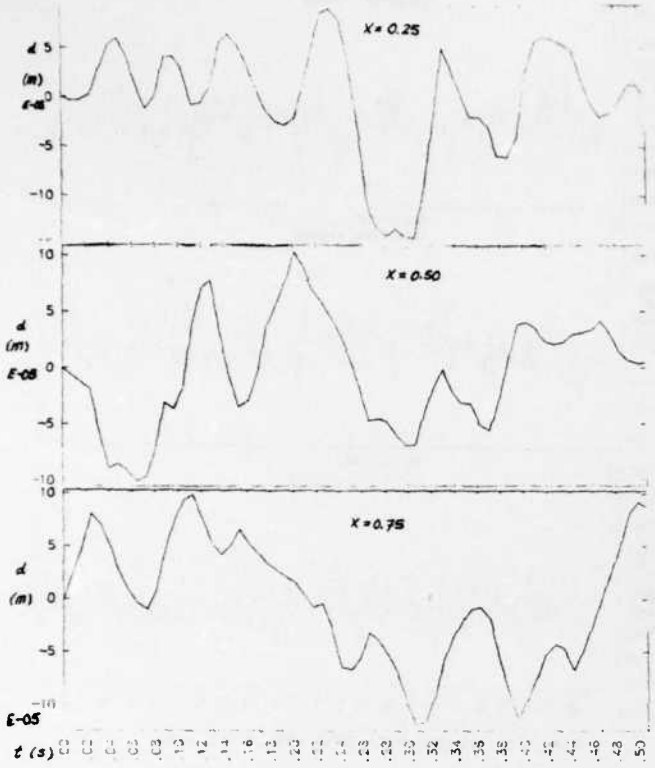

Fig. 9 Surface displacement response at 10 m/s.

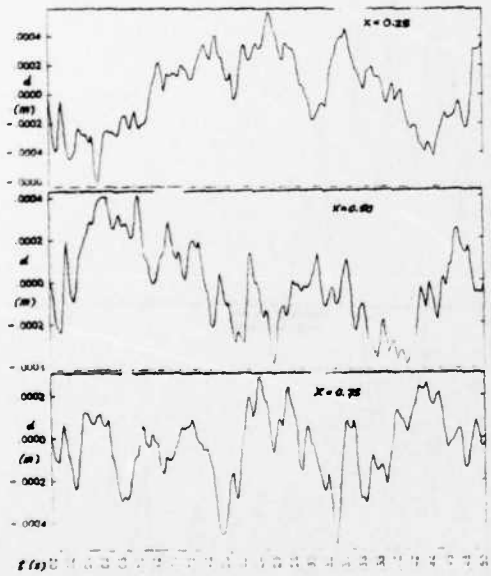

Fig. 10 Surface displacement response at 30 m/s.

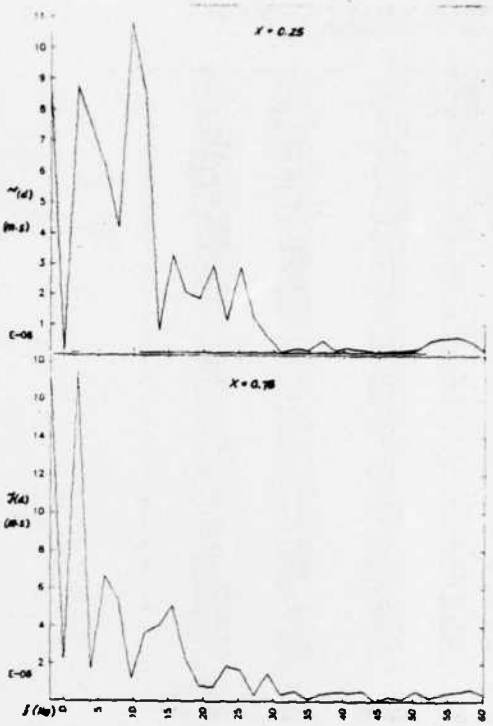

Fig. 11 Surface response spectra at 10 m/s.

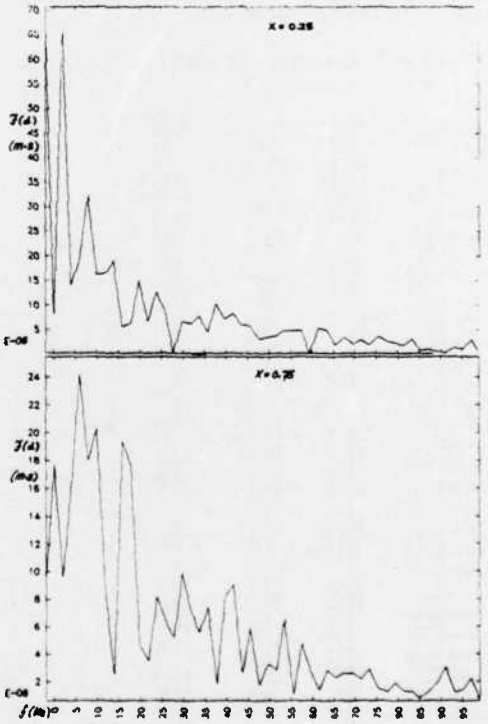

Fig. 12 Surface response spectra at 30 m/s.

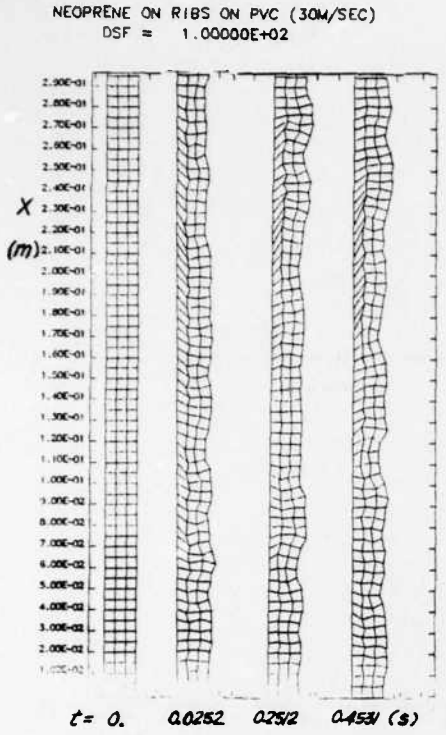

Fig. 13 Internally structured neoprene surface coating deformation at 30 m/s.

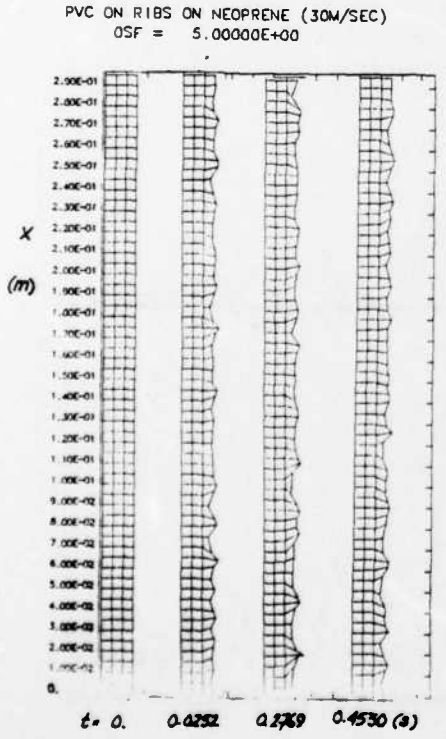

Fig. 14 Internally structured PVC surface coating deformations at 30 m/s.

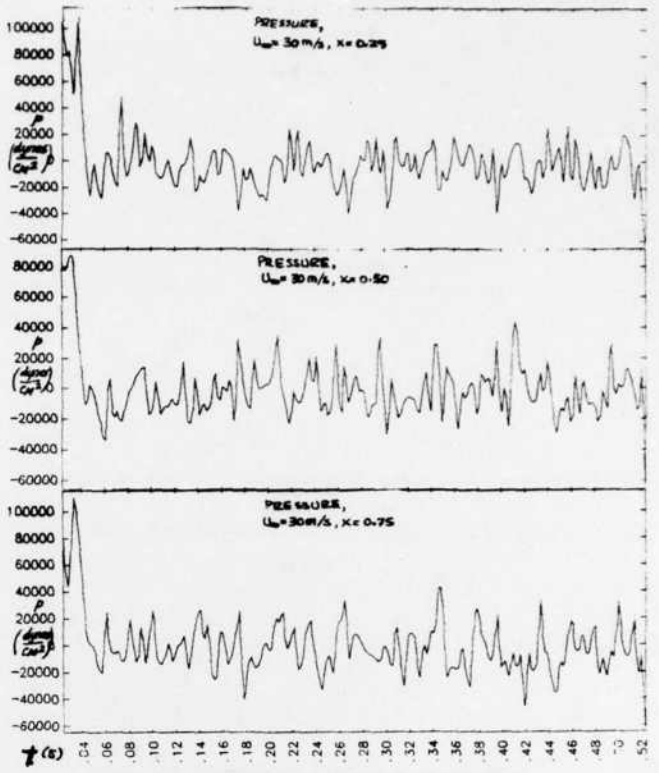

Fig. 15 Turbulent pressure at 30 m/s.

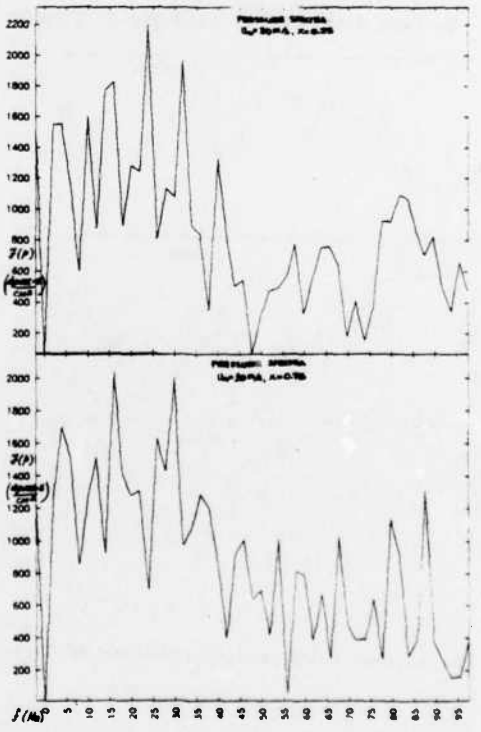

Fig. 16 Turbulent pressure spectra at 30 m/s.

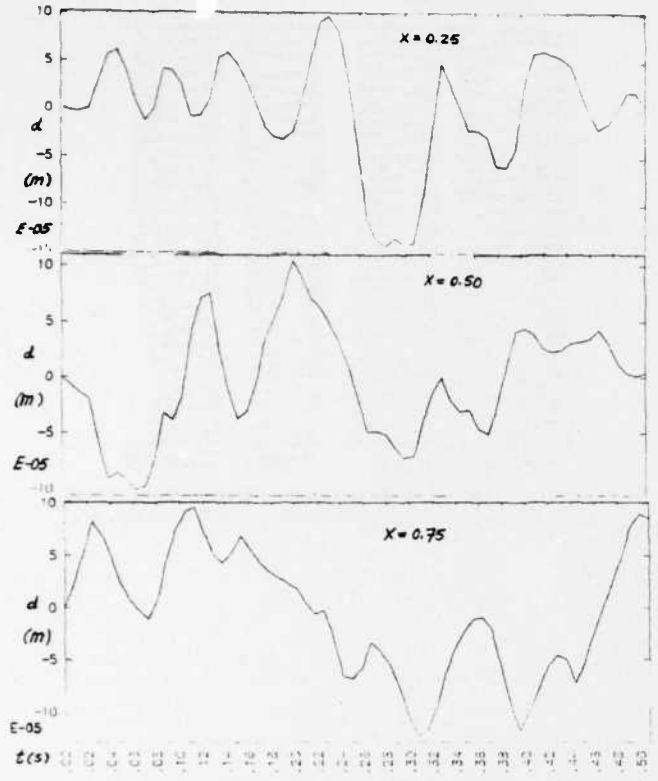

Fig. 17 Internally structured PVC surface coating displacement response at 10 m/s.

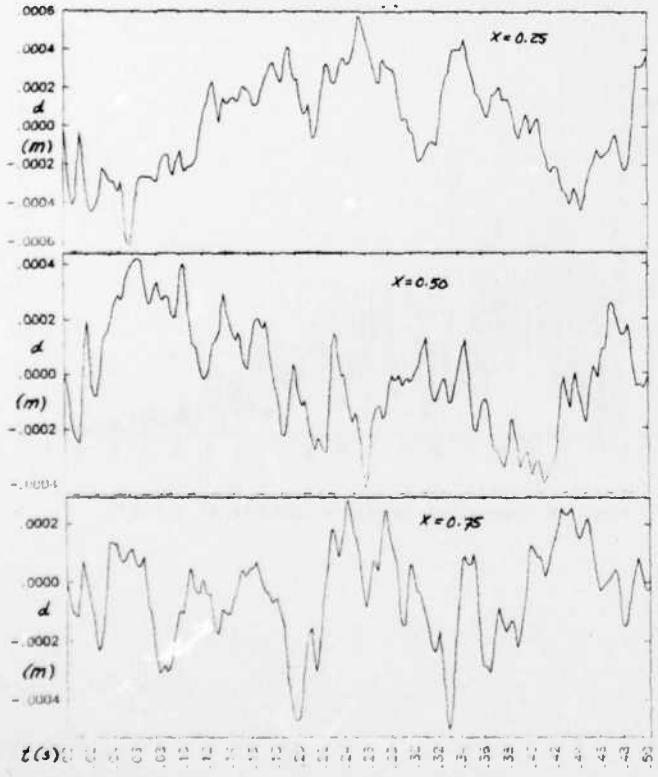

Fig. 18 Internally structured PVC surface coating displacement response at 30 m/s.

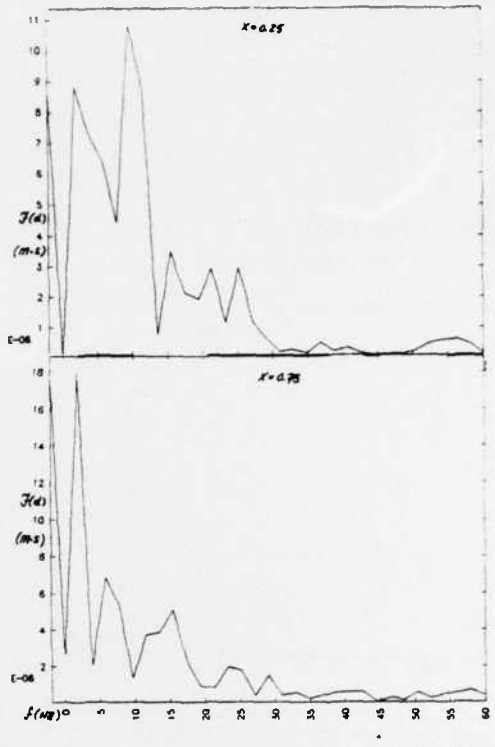

Fig. 19 Internally structured PVC surface coating response spectra at 10 m/s.

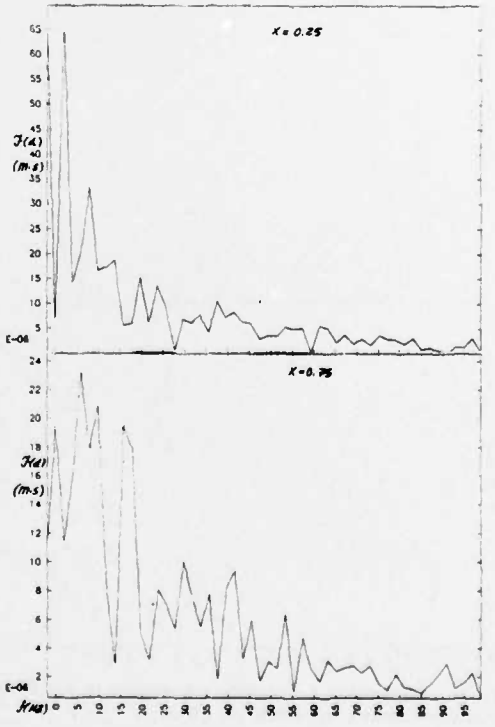

Fig. 20 Internally structured PVC surface coating response spectra at 30 m/s.

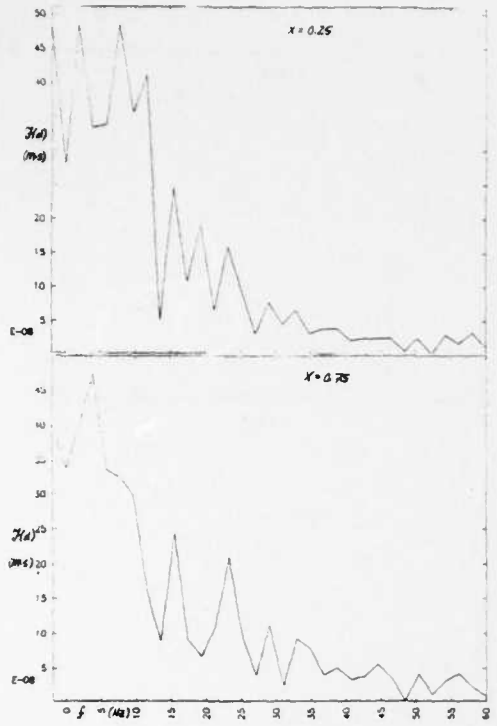

Fig. 21 Internally structured neoprene surface coating response spectra at 10 m/s.

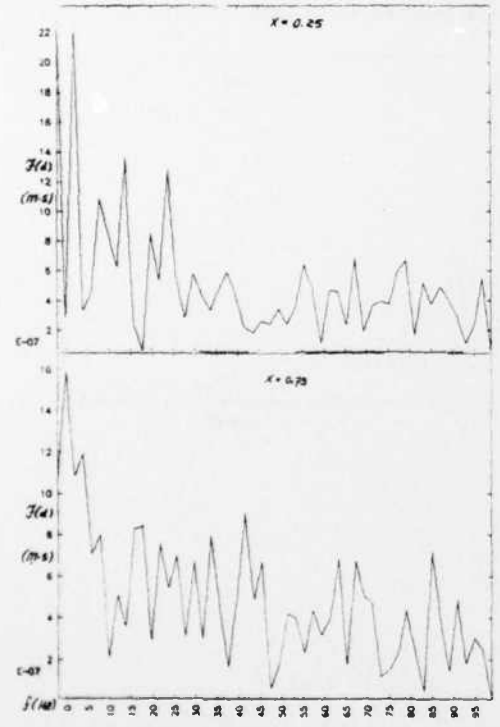

Fig. 22 Internally structured neoprene surface coating response spectra at 30 m/s.

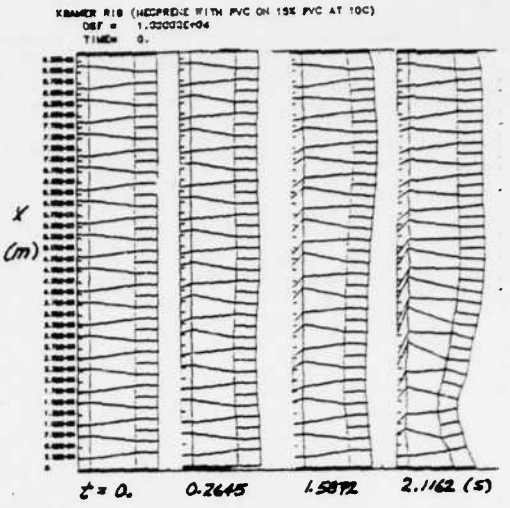

Fig. 23 Internally structured Kramer model small scale coating and modeled surface deformation at 1.5 m/s.

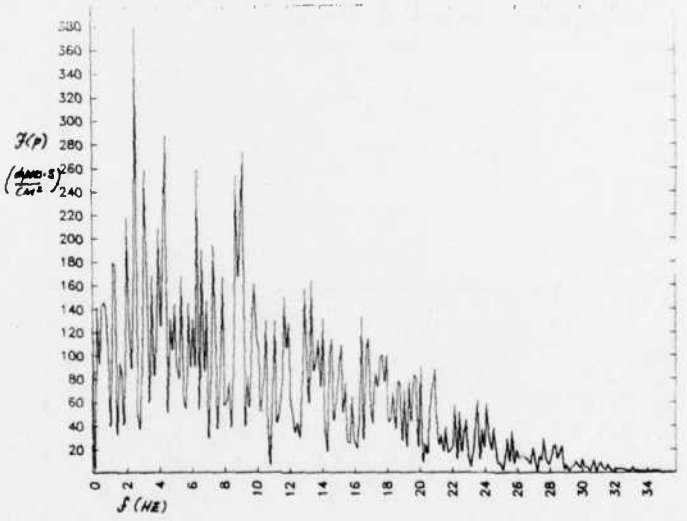

Fig. 24 Turbulent pressure spectra at 1.5 m/s.

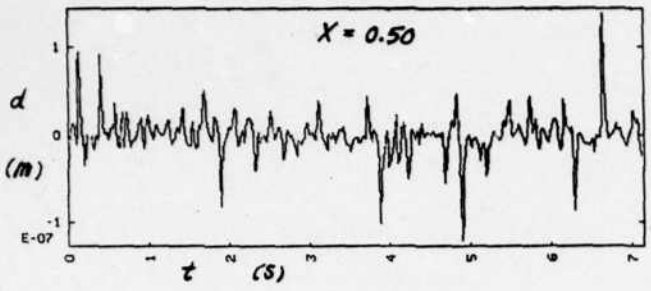

Fig. 25 Internally structured Kramer model small scale coating displacement response at 1.5 m/s.

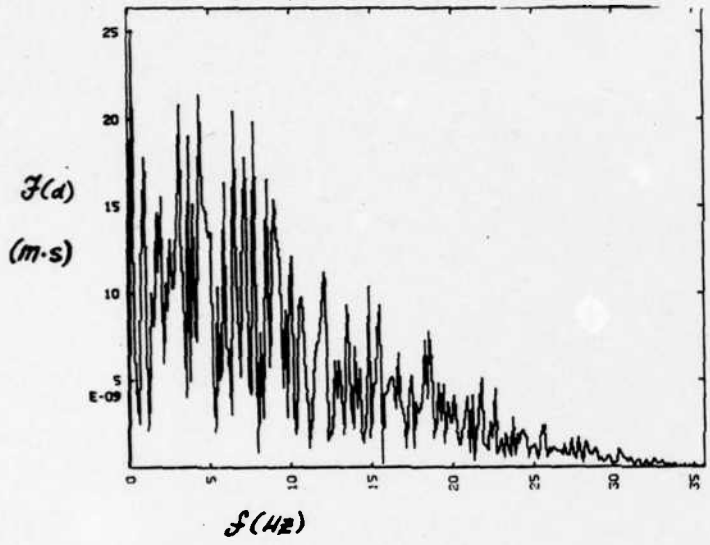

Fig. 26 Internally structured Kramer model small scale coating response spectra at 1.5 m/s.

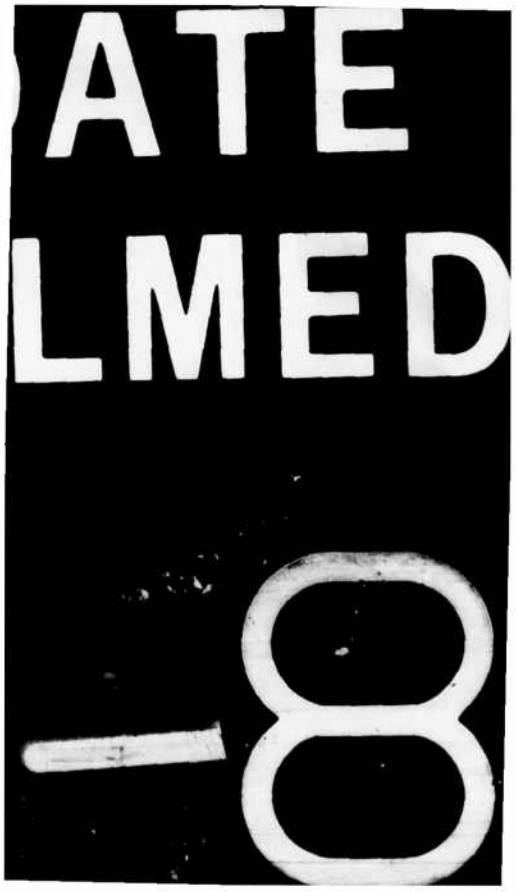
ATE
LMED
8